

Topological Quantum Materials with Kagome Lattice

Qi Wang, Hechang Lei,* Yanpeng Qi,* and Claudia Felser



Cite This: *Acc. Mater. Res.* 2024, 5, 786–796



Read Online

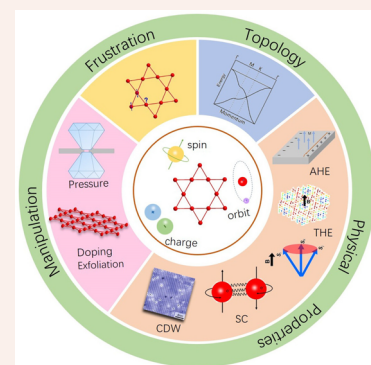
ACCESS |

Metrics & More

Article Recommendations

CONSPECTUS: Recently, various topological states have undergone a spurt of progress in the field of condensed matter physics. An emerging category of topological quantum materials with kagome lattice has drawn enormous attention. A two-dimensional kagome lattice composed of corner-sharing triangles is a fascinating structural system, which could not only lead to geometrically frustrated magnetism but also have a nontrivial topological electronic structure hosting Dirac points, van Hove singularities, and flat bands. Due to the existence of multiple spin, charge, and orbit degrees of freedom accompanied by the unique structure of the kagome lattice, the interplay between frustrated magnetism, nontrivial topology, and correlation effects is considered to result in abundant quantum states and provides a platform for researching the emergent electronic orders and their correlations.

In this Account, we will give an overview of our research progress on novel quantum properties in topological quantum materials with kagome lattice. Here, there are mainly two categories of kagome materials: magnetic kagome materials and nonmagnetic ones. On one hand, magnetic kagome materials mainly focus on the 3d transition-metal-based kagome systems, including Fe_3Sn_2 , $\text{Co}_3\text{Sn}_2\text{S}_2$, YMn_3Sn_6 , FeSn , and CoSn . The interplay between magnetism and topological bands manifests vital influence on the electronic response. For example, the existence of massive Dirac or Weyl fermions near the Fermi level significantly enhances the magnitude of Berry curvature in momentum space, leading to a large intrinsic anomalous Hall effect. In addition, the peculiar frustrated structure of kagome materials enables them to host a topologically protected skyrmion lattice or noncoplanar spin texture, yielding a topological Hall effect that arises from the real-space Berry phase. On the other hand, nonmagnetic kagome materials in the absence of long-range magnetic order include CsV_3Sb_5 with the coexistence of superconductivity, charge density wave state, and band topology and van der Waals semiconductor $\text{Pd}_3\text{P}_2\text{S}_8$. For these two kagome materials, the tunability of electric response in terms of high pressure or carrier doping helps to reveal the interplay between electronic correlation effects and band topology and discover the novel emergent quantum phenomena in kagome materials.



1. INTRODUCTION

Recently, topological quantum materials that host nontrivial topological states have become a hot frontier in condensed matter systems. Various intriguing topological states have been predicted theoretically and observed experimentally, including topological insulators, Dirac and Weyl semimetals, etc.^{1,2} Topological insulators are characterized by an insulated bulk state with topologically protected conductive boundary/surface states. Dirac and Weyl semimetals belong to topological semimetals, which are a new class of topological quantum states featuring gapless band crossings of linear dispersion in the vicinity of the Fermi level. Dirac fermions that satisfy the Dirac equation are 4-fold degenerate and further break spatial-inversion or time-reversal symmetry, and 2-fold degenerate Weyl fermions appear in pairs and have opposite chirality. In topological quantum materials, owing to the intriguing nontrivial topological band structure, many fascinating properties have been observed, such as extremely large magneto-resistance, chiral anomaly and surface-state Fermi arcs, etc.

Topological quantum materials with kagome lattice have now become an emerging class of topological materials

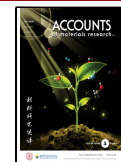
systems. A two-dimensional (2D) kagome lattice is geometrically defined as corner-sharing triangles, hosting a strong geometric frustration effect (Figure 1a). In the case of the antiferromagnetic Heisenberg model on a triangle sublattice, there is no unique ground state that can simultaneously satisfy the antiferromagnetic correlation interactions, leading to the emergence of spin disorder or strong quantum fluctuation. Due to the peculiar structural configuration, kagome lattice has been expected to be one of candidate systems to realize exotic quantum states, such as quantum spin liquid state. Moreover, with a decrease in the degree of degeneracy of the ground state, a noncollinear/coplanar spin frustrated configuration in kagome lattice is permitted to exist. In the view of electronic structure, considering the nearest electron hopping based on

Received: December 30, 2023

Revised: May 8, 2024

Accepted: May 8, 2024

Published: June 20, 2024



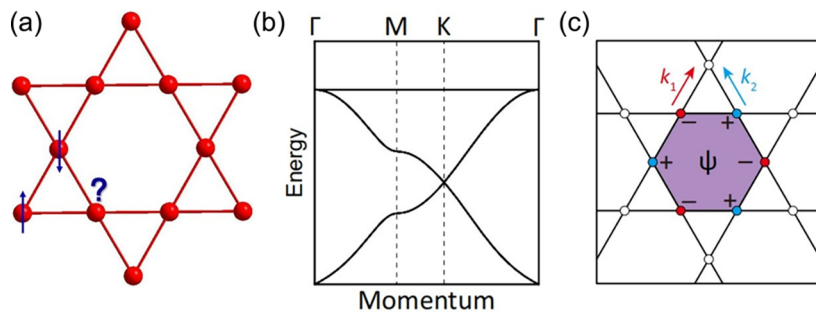


Figure 1. (a) The geometrical structure of 2D kagome lattice. The blue arrows and question mark on a triangular sublattice denote the frustrated configuration. (b) Topological band structure of kagome lattice in consideration of the nearest electron hopping without SOC. (c) The schematic of destructive interference of Bloch wave functions (ψ) in kagome lattice. (b–c) Reproduced with permission from ref 3. Copyright 2021 Nature.

the tight-binding model in the absence of spin orbit coupling (SOC), the electronic band structure along high symmetry directions accordingly gives rise to three nontrivial energy bands (Figure 1b).³ Two of them are similar to the case in honeycomb lattice, where 2-fold degenerate bands cross linearly at the K point in momentum space, generating a 4-fold degenerate Dirac point. The third band with zero bandwidth exhibits a dispersionless feature in the entire Brillouin zone (BZ), commonly referred to as a flat band. It is generated by the destructive interference of Bloch wave functions in the case of nearest electron hopping (Figure 1c), where the Bloch electrons localized within the hexagon of the kagome lattice possess fully quenched kinetic energy and Coulomb interactions dominate. The flat band and Dirac band touch and degenerate at the Γ point. Furthermore, two van Hove singularities in the Dirac band are formed at the M point.

The nontrivial topological characteristics and topological magnetic excitations are expected to play a vital role on the electronic response. Generally, the measurement of the Hall effect has become a crucial means to characterize the electromagnetic response of conduction electrons in metallic materials. After Edwin H. Hall first discovered the normal Hall effect (NHE) in 1879,⁴ which arises from the transverse motion of carriers caused by the Lorentz force, an additional large contribution of resistivity related to spontaneous magnetization was revealed in ferromagnetic metals two years later, known as the anomalous Hall effect (AHE).^{5,6} The Hall resistivity can be described by the empirical formula,

$$\rho_{xy} = \rho_{xy}^N + \rho_{xy}^A = R_0 B + R_s \mu_0 M \quad (1)$$

where the ordinary Hall coefficient R_0 determines the concentration and type of apparent carriers and R_s corresponds to the anomalous Hall coefficient, which is usually much larger than R_0 .

Up to now, it is generally admitted that the intrinsic or extrinsic mechanism (side jump scattering and skew scattering) could account for the physical origin of AHE. On one hand, the intrinsic mechanism first proposed by Karplus and Luttinger is considered to be exclusively relevant to the inherent band structure of the material.⁷ Later, one can understand the intrinsic AHE in the view of the Berry curvature effect.⁸ The anomalous Hall conductivity (AHC) σ_{xy}^A can be determined by integrating the Berry curvature (Ω) of all the occupied bands below the Fermi level (E_F):

$$\sigma_{xy}^A = -\frac{2\pi e^2}{h} \int_{BZ} \frac{d^3k}{(2\pi)^3} \sum_n f_n(k) \Omega_n^z(k),$$

where h and $f_n(k)$ are the Plank constant and the Fermi–Dirac distribution function,

respectively. Therefore, AHE should be observed in a system with time-reversal symmetry broken that hosts a nonzero Berry curvature. The intrinsic AHC manifests the maximum magnitude of e^2/ha (10^2 – 10^3 Ω^{-1} cm^{-1}) in the three-dimensional (3D) condition when E_F is within the energy gap, where a is the lattice constant. In particularly, for kagome topological semimetals with broken time-reversal symmetry, the massive Dirac points with Chern gaps in the condition of Kane–Mele-type SOC or magnetic Weyl points will greatly enhance the magnitude of Berry curvature when the topologically protected linear band crossings are close to E_F , contributing to a large intrinsic AHE. On the other hand, extrinsic mechanisms are interpreted as arising from the impurity-induced asymmetrical spin scattering in the presence of spin–orbit interaction (SOI).^{9,10} Generally, the extrinsic contribution is inescapable and usually coexists with intrinsic contribution in real materials.

In addition to the effects of Berry curvature in momentum space, for noncoplanar spin texture such as the topologically protected skyrmions state or noncoplanar magnetic structure with nonzero scalar spin chirality $\chi_{ijk} = S_i \cdot (S_j \times S_k)$ (where S_i , S_j , and S_k are the three nearest spins), a real-space Berry phase can be obtained when the Bloch electrons cross the peculiar magnetic structure. Correspondingly, a fictitious magnetic field similar to the role of an extrinsic magnetic field in NHE emerges and generates a topological Hall effect (THE).¹¹ In magnetic kagome materials, the natural frustrated structure offers potentialities to realize magnetic excitations and THE.

Moreover, van Hove singularities and flat bands in kagome lattice both contribute to a large density of states (DOS), which could lead to strong electron correlation effects. This is in contrast with Dirac fermions, which make no contribution to DOS. Diverse correlated electronic states including superconductivity and ferromagnetism as well as Wigner crystal are predicted in the flat band model. Additionally, when the time-reversal symmetry is broken when considering SOC, a topological flat band analogous to the Landau level possesses a nonzero Chern number. It could give rise to a fractional quantum Hall effect at partial filling at high temperature (even room temperature).¹² With regard to van Hove singularities, the various electronic ground states like superconductivity or spin/charge density wave (CDW) can be realized at van Hove filling concomitant with varying Coulomb interactions.¹³

This Account mainly focuses on the topological quantum materials that feature kagome lattice composed of diverse 3d/4d transition metal atoms. According to our research results on the electrical transport responses combined with theoretical

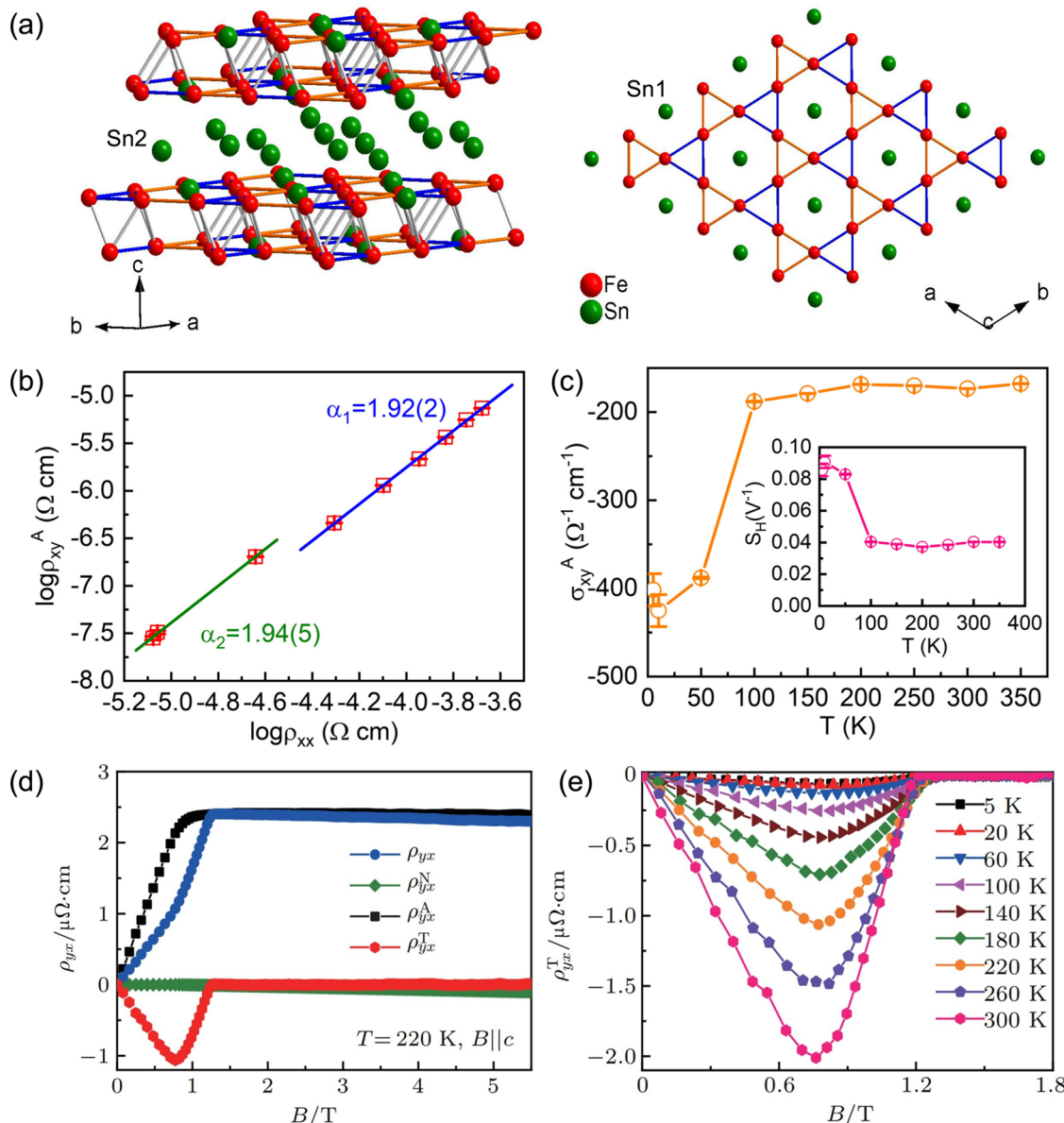


Figure 2. (a) The crystal structure of Fe_3Sn_2 . (b) Scaling relationship between ρ_{xy}^A and ρ_{xx} in an Fe_3Sn_2 single crystal. (c) Temperature dependence of $\sigma_{xy}^A(T)$. The inset denotes the $S_H(T)$ curve. (d) Field-dependent $\rho_{yx}(B)$, $\rho_{yx}^A(B)$, and $\rho_{yx}^T(B)$ at 220 K for $B \parallel c$. (e) $\rho_{yx}^T(B)$ as a function of field between 5 and 300 K. Reproduced with permission from refs 14 and 20. Copyright 2016 APS and 2020 IOP.

calculations and spectroscopy experiments, this Account will be described in four parts. In the first part, we provide an overview of the fundamental properties of kagome lattice as well as the correlated electromagnetic responses including AHE and THE. In the second and third parts, we will systematically introduce our research progress regarding the novel quantum properties in a series of representative topological kagome materials, consisting of magnetic kagome materials Fe_3Sn_2 , $\text{Co}_3\text{Sn}_2\text{S}_2$, YMn_6Sn_6 , FeSn , and CoSn as well as nonmagnetic kagome materials CsV_3Sb_5 and $\text{Pd}_3\text{P}_2\text{S}_8$. The last part will give a brief conclusion and perspective of topological kagome materials.

2. MAGNETIC KAGOME MATERIALS

2.1. Fe_3Sn_2

The first case of kagome magnets is the ferromagnet Fe_3Sn_2 with a Curie temperature $T_c \approx 640$ K.¹⁴ For the crystal

structure, the bilayer kagome lattice composed of Fe atoms is sandwiched between Sn₂ honeycomb layers along the c -axis (Figure 2a). Sn₁ atoms are located in the centers of hexagons in each monolayer kagome lattice. The study of neutron powder diffraction revealed that there is a spin reorientation process in Fe_3Sn_2 where Fe spins tilt from the c -axis to the ab -plane upon reducing temperature.¹⁵ It has also been reflected in magnetic susceptibility curves, accompanying a plateau at low temperature under $H \parallel ab$, indicating the almost accomplishment of spin reorientation.¹⁴

The Hall resistivity curves $\rho_{xy}(B)$ show the analogous shapes to those of $M(B)$, which display typical ferromagnetic characteristics, suggesting the presence of AHE. In accordance with formula 1, the negative R_0 yielded by the fitted slope of $\rho_{xy}(B)$ in the saturated field region demonstrates that the dominant carriers are electrons. As shown in Figure 2b, the near-quadratic scaling relation between ρ_{xy}^A and ρ_{xx} demon-

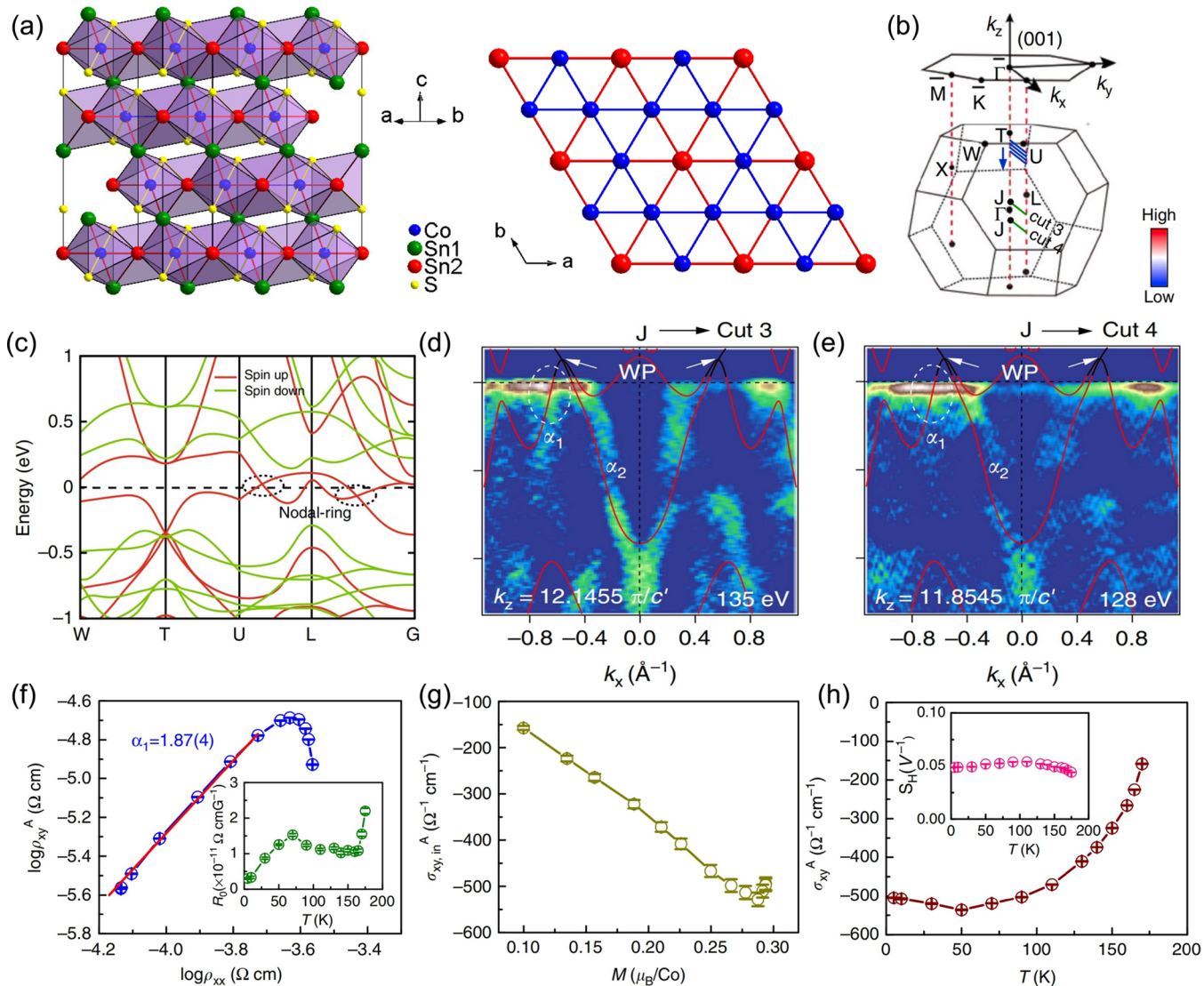


Figure 3. (a) Crystal structure of $\text{Co}_3\text{Sn}_2\text{S}_2$. (b) The schematic of 3D and 2D projected BZ. (c) The calculated band structure without spin orbit coupling. (d and e) ARPES spectra along cuts 3 and 4 of the $\text{Co}_3\text{Sn}_2\text{S}_2$ single crystal and the corresponding theoretical calculations (red lines). (f) $\log \rho_{xy}^A(T)$ versus $\log \rho_{xx}^A(T)$; the inset is the $R_0(T)$ curve. (g) M dependence of $\sigma_{xy,in}^A$. (h) Temperature dependence of σ_{xy}^A . Reproduced with permission from ref 25. Copyright 2018 Nature.

strates that the intrinsic or extrinsic side-jump mechanism instead of skew scattering ($\rho_{xy}^A \propto \rho_{xx}$) is responsible for the AHE. Extraordinarily, it is found that σ_{xy}^A ($\approx -\rho_{xy}^A/\rho_{xx}^2 = -R_0 M/\rho_{xx}^2$) shows large value and approaches $-400 \Omega^{-1} \text{ cm}^{-1}$ when the temperature drops below 100 K (Figure 2c). In theory, the contribution of side-jump scattering [$\sigma_{xy,sj}^A$] could be estimated by means of $(e^2/h)(\epsilon_{SO}/E_F)$, where ϵ_{SO} is spin-orbit interaction. The ratio of ϵ_{SO} to E_F is generally less than 10^{-2} , which would lead to a rather small AHE. Hence, the main contribution of AHE should arise from the intrinsic mechanism. Specially, the temperature-independent $S_H (\mu_0 R_s / \rho_{xx}^2 = -\sigma_{xy}^A/M)$ also confirmed the intrinsic origin (inset of Figure 2c). Furthermore, in 2018, the study of angle-resolved photoemission spectroscopy (ARPES) by Checkelsky's group revealed that there are massive Dirac fermions with a gap of 30 meV near E_F in Fe_3Sn_2 due to SOC and the Berry curvature is enormously enhanced, contributing to a large AHC.¹⁶

Generally, magnetic skyrmions induced by Dzyaloshinskii-Moriya interactions are commonly observed in noncentrosymmetric systems, like B20 chiral magnets.¹⁷ Recently, the

existence of skyrmions has been extended into centrosymmetric magnetic materials, especially for the frustrated magnets where skyrmions are stabilized by magnetic frustration interactions.¹⁸ Interestingly, Lorentz transmission electron microscopy (LTEM) reported the presence of field-induced skyrmionic bubbles in centrosymmetric frustrated Fe_3Sn_2 over a wide temperature range from 100 to 400 K.¹⁹ Moreover, it is noticed that the slopes between $\rho_{yx}(B)$ and $M(B)$ below the saturated field exhibit a slight difference, suggesting the possible additional contribution of THE to Hall resistivity.²⁰ Considering the topological Hall component, the Hall resistivity can be further expressed in three parts:

$$\rho_H = \rho_H^N + \rho_H^A + \rho_H^T = R_0 B + S_H \rho^2 M + \rho_H^T \quad (2)$$

where ρ_H^T is the topological Hall resistivity. From the analyses of scaling curves, the component of THE is undoubtedly obtained below 1.3 T within a wide temperature region (5–300 K), as shown in Figures 2d and 2e. The monotonically varying ρ_H^T possesses a giant topological Hall response with a

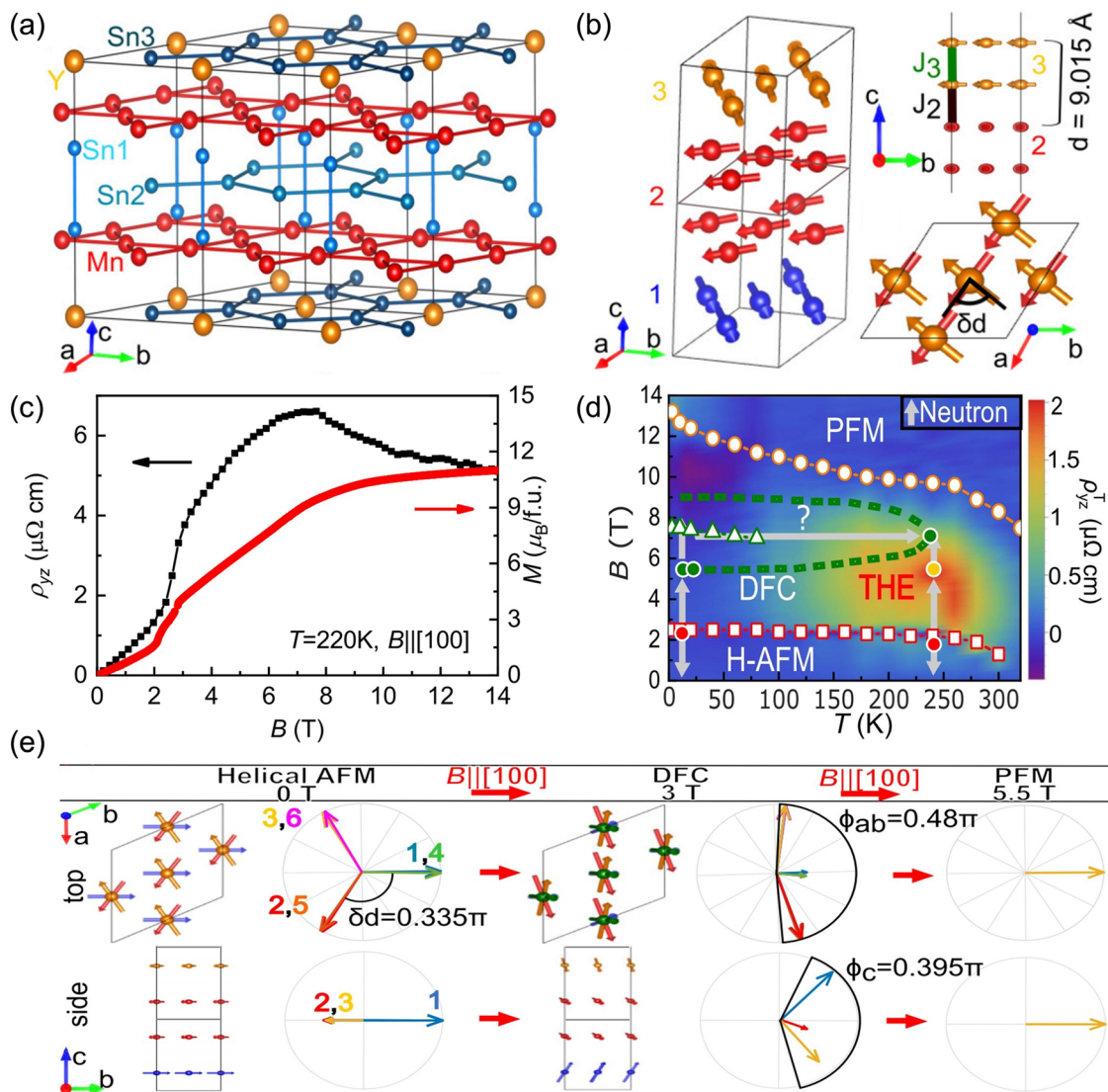


Figure 4. (a and b) Crystal structure (left) and zero-field magnetic structure (right) of YMn_6Sn_6 . d displays the distance between the nearest kagome bilayer. J_2 and J_3 represent the magnetic exchange couplings in adjacent layers. (c) Field-dependent Hall resistivity $\rho_{yz}(B)$ and $M(B)$ in the field of the $[100]$ direction. (d) Phase diagram along the $[100]$ direction field. YMn_6Sn_6 undergoes a helical antiferromagnetic (H-AFM) structure, a double-fan structure with a c -axis component (DFC), and a polarized ferromagnetic (PFM) structure under magnetic field. (e) Magnetic structure model of YMn_6Sn_6 at a temperature of 240 K . Reproduced with permission from ref 30. Copyright 2021 APS.

maximum absolute value of $2.01\text{ }\mu\Omega \text{ cm}$ at 300 K . The magnitude is comparable with that in centrosymmetric Gd_2PdSi_3 ($2.6\text{ }\mu\Omega \text{ cm}$ at 2 K) with skyrmion lattice,¹⁸ significantly larger than those in previous reported skyrmionic B20 materials like MnSi ($4\text{ n}\Omega \text{ cm}$).¹⁷ The estimated helical period in view of skyrmionic bubbles is found to be 8.8 nm , which is considerably smaller than that ($\sim 500\text{ nm}$) observed in LTEM. Considering the presence of spin reorientation that could generate noncollinear magnetic structure, it can be concluded that the synergistic effect of noncollinear spin texture and skyrmion structure is possibly responsible for the giant THE. On the other hand, above the field of 1.3 T , THE disappears owing to the full polarization of Fe spins toward the field, then intrinsic AHE dominants in the Hall response (Figure 2d).

Furthermore, a neutron scattering study revealed that the in-plane local magnetism in Fe_3Sn_2 can be efficiently regulated by small magnetic fields, generating a pronounced electromagnetic response that shows anisotropic magnetoresistance

(MR) under varying in-plane magnetic fields.²¹ Additionally, Zeng et al. confirmed the existence of flat bands below E_F about 0.2 eV by utilizing ARPES.²²

2.2. $\text{Co}_3\text{Sn}_2\text{S}_2$

Various kinds of topological semimetals have been discovered by means of experiments and theories, while the studies on magnetic Weyl semimetals with breaking time-reversal symmetry make relatively slow progress. HgCr_2Se_4 and $\text{Y}_2\text{Ir}_2\text{O}_7$ were predicted to host magnetic Weyl fermions in the early theoretical calculations^{23,24} but have not yet been confirmed experimentally. Due to the existence of magnetic interactions and the Weyl fermions being generally located away from the E_F in real materials, the realizations of magnetic Weyl fermions and the corresponding electromagnetic response are challenging. Consequently, the search for magnetic Weyl fermions has remained stagnant. The breakthrough in magnetic Weyl semimetals stems from the

discovery of half-metallic ferromagnet $\text{Co}_3\text{Sn}_2\text{S}_2$, found independently by Lei's group and Felser's group.^{25,26}

$\text{Co}_3\text{Sn}_2\text{S}_2$ features a Co kagome layer in which Sn2 atoms are situated in the centers of hexagons (Figure 3a). It experiences a ferromagnetic transition at $T_c \approx 174$ K and displays a soft ferromagnetic behavior characterized by a small coercive field of 0.08–0.1 T. Due to the half-metallic feature, $\text{Co}_3\text{Sn}_2\text{S}_2$ manifests a full polarization of spins toward one direction. The 3d orbitals of Co atoms mainly contribute to the bands close to E_F , which form a nodal ring around the L point in the absence of SOC (Figure 3c). When introducing SOC, three pairs of Weyl points with opposite chirality located at 50 meV above E_F and away from the high-symmetry directions are obtained. On the other hand, ARPES experiments were performed to characterize the electronic structure in $\text{Co}_3\text{Sn}_2\text{S}_2$. There is a trend of linear dispersion between the α_1 and α_2 bands above E_F along cuts 3 and 4 (Figures 3d and 3e). The consistency between the ARPES results and theoretical calculations confirms the existence of Weyl fermions in $\text{Co}_3\text{Sn}_2\text{S}_2$.

It is reported that the Weyl fermions in magnetic Weyl semimetals acting as magnetic monopoles in momentum space can make vital contributions to Berry curvature. It can lead to the remarkable transport response like huge AHE, and thus we carried out the transport measurements on single crystal $\text{Co}_3\text{Sn}_2\text{S}_2$. The hole-type carriers are dominant in $\text{Co}_3\text{Sn}_2\text{S}_2$ due to the positive R_0 (inset of Figure 3f). As shown in Figure 3f, ρ_{xy}^A almost scales quadratically with ρ_{xx} at low temperatures, which first excludes the contribution of skew scattering. On the other hand, the intrinsic contribution under various temperatures can be extracted by the scaling curves of $\rho_{xy}^A/(\rho_{xx}M)$ versus ρ_{xx} according to the formula $\rho_{xy}^A = a(M)\rho_{xx} + b(M)\rho_{xx}^2$. Consequently, a remarkably large intrinsic AHC $|\sigma_{xy,in}^A|$ was obtained, reaching a value as much as $505 \Omega^{-1} \text{ cm}^{-1}$ at low temperature (Figure 3g). Moreover, the $\sigma_{xy,in}^A$ depends linearly on magnetization, which is well consistent with the results of theoretical calculations. By contrast, the estimated $|\sigma_{xy,sj}^A|$ only contributes a small magnitude of $3.9 \Omega^{-1} \text{ cm}^{-1}$. Another intrinsic feature is the temperature-independent behavior of σ_{xy}^A and S_H (Figure 3h). Moreover, the $|\sigma_{xy}^A|$ decreases gradually when $T > 140$ K, which primarily arises from the obvious reduction in $M(T)$ near T_c . The scaling analyses confirm that the striking AHE is dominated by an intrinsic mechanism. Combined with the first-principles calculations and ARPES, the large intrinsic AHC emerged in $\text{Co}_3\text{Sn}_2\text{S}_2$ is closely related to the presence of magnetic Weyl fermions close to E_F . Later on, the observations of Fermi arcs and related phenomena by using ARPES and scanning tunneling microscopy (STM) in other research groups further confirm the existence of Weyl fermions in ferromagnetic $\text{Co}_3\text{Sn}_2\text{S}_2$.^{27,28} In addition, a giant anomalous Hall angle (20%) and negative MR associated with the chiral anomaly of Weyl fermions have also been observed.²⁶

Regarding the physics of the flat band in $\text{Co}_3\text{Sn}_2\text{S}_2$, STM measurements demonstrate a sharp peak in both the dI/dV spectra on S and the side surface below E_F , which arises from the contribution of the flat band in kagome lattice.²⁹ The peak shows a positive energy shift under magnetic fields, which is distinct from the conventional Zeeman effect, ascribing to the negative orbital magnetism of the flat band. These experimental studies deepen the understanding of magnetic Weyl semimetals significantly.

2.3. YMn₆Sn₆

The centrosymmetric antiferromagnet YMn₆Sn₆ belongs to the RMn₆Sn₆ (R = rare earth elements) kagome family with space group $P6/mmm$. In contrast to the crystal structures of the kagome magnets Fe₃Sn₂ and Co₃Sn₂S₂ where Sn atoms are located in the kagome layer, the occupation of R atoms in R–Sn3 layer leads to the displacement of Sn1 atoms out of the Mn kagome layer, resulting in the emergence of a clean Mn kagome lattice (Figure 4a).³⁰ The family exhibits multiple magnetic ground states by varying R elements, like ferrimagnets RMn₆Sn₆ (R = Gd–Ho), and antiferromagnets ErMn₆Sn₆ and YMn₆Sn₆.^{30,31} In YMn₆Sn₆, the magnetization only arises from the contribution of Mn atoms. The Mn spins in each kagome bilayer (Mn–Sn1–Sn2–Sn1–Mn sheets) are in a linear ferromagnetic arrangement without the *c*-axis component and collectively rotate δd degree to the adjacent kagome bilayer (Figure 4b), i.e., YMn₆Sn₆ exhibits a helical antiferromagnetism ($T_N \approx 333$ K). When applying field along the *ab*-plane, a spin–flop transition appears around 2.5 T below 300 K.

From the measurements of Hall resistivity, it is found that the carrier densities of electrons and holes change when applying fields along *ab*-plane and *c*-axis, reflecting the obvious influence of field on the electrical structure. The relatively large intrinsic AHE was realized in YMn₆Sn₆ for both field directions based on the scaling analyses between ρ_H/B and $\rho^2 M/B$ and the weak dependence of σ_{xy}^A on longitudinal conductivity, featuring 45 S cm^{-1} for σ_{xy}^A and 300 S cm^{-1} for σ_{zy}^A . These values are comparable with that in ferrimagnetism TbMn₆Sn₆ ($121 \pm 6 \Omega^{-1} \text{ cm}^{-1}$).³² The Chern-gapped Dirac fermions realized by ARPES experiments,³³ as also discovered in TbMn₆Sn₆ via STM, contribute to the large intrinsic AHC.

Moreover, it is noticed that an obvious difference between $\rho_H(B)$ and $M(B)$ exists below the fully spin polarized region. The signals of THE were obtained in different field directions after subtracting the NHE and AHE components. Surprisingly, the THE is larger when the field is parallel to the kagome plane, reaching a maximum ρ_{yz}^T of $2.0 \mu\Omega \text{ cm}$ at 5 T and 240 K, whereas ρ_{yx}^T is relatively small with a maximum value of $-0.28 \mu\Omega \text{ cm}$ for the *c*-axial field of 5 T at 220 K. For the microscopic mechanism of the field-direction-dependent large THE, small-angle neutron scattering experiments first exclude the existence of skyrmion lattice in YMn₆Sn₆. A phase diagram, which integrates the magnetic structures determined by neutron diffraction and the topological Hall response ρ_{yz}^T , is depicted in Figure 4d. For the *ab*-plane magnetic field, the Mn spins in the helical antiferromagnetic (H-AFM) structure are initially located in the kagome plane, yielding a small contribution to THE. Above the spin–flop transition field, a field-driven double-fan phase with a *c*-axis component (DFC) emerges (Figure 4e), generating a large nonzero spin chirality χ which is essential to the significant THE. The specific spin texture manifests exclusively in the case of the comparability of *c*-axis AFM exchange couplings and in-plane interactions. THE finally disappears in the fully polarized ferromagnetic (PFM) state at high field, and then the intrinsic AHE dominates in YMn₆Sn₆. By contrast, the small ρ_{yx}^T for $H \parallel c$ could be related to the noncollinear magnetic structure formed during the process that causes the in-plane Mn spin to progressively align toward the *c*-axis direction. In addition, for the characterization of the electronic structure, the flat band and saddle point near E_F were confirmed by ARPES.³³

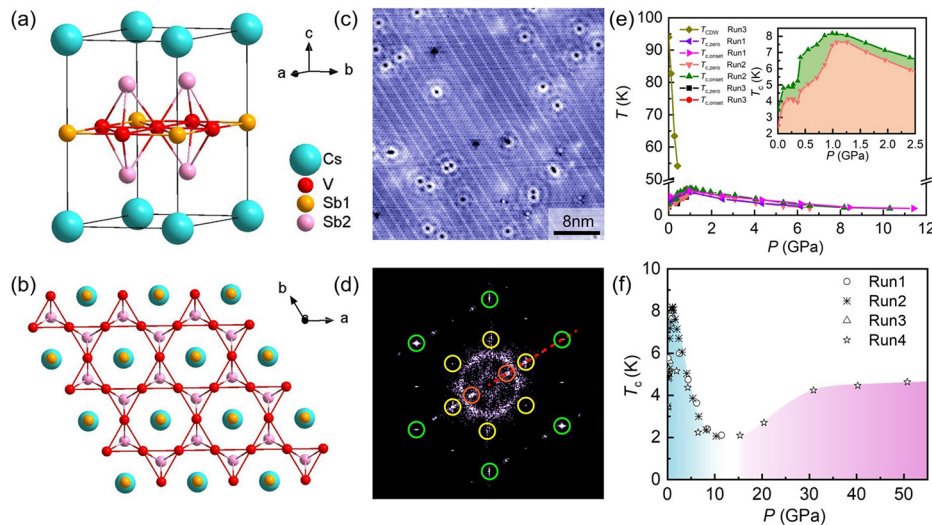


Figure 5. (a and b) Crystal structure of CsV_3Sb_5 . (c) High-resolution STM topography of Sb-terminated surface. (d) The corresponding Fourier transform. The green, yellow, and orange circle symbols denote Q Bragg peaks, Q_{2a} and Q_{4a} CDW vectors, respectively. (e and f) Phase diagrams of temperature (T_c and T_{CDW}) and pressure (P) in CsV_3Sb_5 . Reproduced with permission from ref 42. Copyright 2021 Wiley.

Another representative Mn-based kagome magnet is the antiferromagnetic Weyl semimetal Mn_3Sn , which shows a noncollinear magnetic order with in-plane 120° Mn spins. Nakatsuji's group reported a large intrinsic AHE by electrical transport experiments.³⁴ In addition, the chiral anomaly associated with Weyl fermions was also observed.³⁵

2.4. FeSn and CoSn

FeSn and CoSn feature an isostructural crystal structure with space group $P6/mmm$, which is equivalent to turning the bilayer kagome lattice in Fe_3Sn_2 into a single Fe/Co kagome layer. However, there are different magnetic ground states in them. FeSn exhibits an antiferromagnetism with the *c*-axis antiferromagnetic and *ab*-plane ferromagnetic spin configurations. But for CoSn, it shows a Pauli paramagnetism. No anomalous electromagnetic responses emerged in both FeSn and CoSn. Interestingly, spectroscopic measurements revealed exotic quantum states and correlation effects.^{36–38} The coexistence of Dirac fermions and flat bands has been discovered via ARPES experiments in FeSn and CoSn.^{36,37} In CoSn, the STM measurements demonstrated that the fermion–boson many-body interaction is driven by electrons coupling with the phonon flat band in the Co kagome lattice.³⁸ The evolution of spin excitations was revealed in FeSn and CoSn via inelastic neutron scattering experiments.³

3. NONMAGNETIC KAGOME MATERIALS

3.1. CsV_3Sb_5

Superconductivity is a long-term research hotspot in condensed matter physics. Especially when a system simultaneously hosts superconducting and topological characteristics, more exotic quantum effects could emerge, such as topological superconductivity, Majorana zero modes, etc. Although theoretical predictions suggest the existence of superconductivity in kagome systems, the experimental studies on the superconductivity are still lacking. Until recently, the discoveries of the AV_3Sb_5 ($\text{A} = \text{K}, \text{Rb}, \text{Cs}$) family containing V kagome lattice have greatly advanced the study of superconductivity in kagome materials.^{39–41} The crystal structure of AV_3Sb_5 consists of alternating $\text{A}-\text{Sb}_2-\text{VSb}_1-\text{Sb}_2-\text{A}$ layers,

as shown in Figures 5a and 5b. These compounds, as distinct from the 3d transition-metal-based kagome magnets, have no magnetic order. Especially, they are rare kagome materials that simultaneously possess superconductivity ($T_c \approx 0.92\text{--}2.5$ K) and CDW states ($T_{\text{CDW}} \approx 80\text{--}110$ K) as well as a Z_2 topological band structure. Subsequently, a large number of experimental and theoretical works were carried out on AV_3Sb_5 .

Taking CsV_3Sb_5 as an example,⁴² a $2\text{a} \times 2\text{a}$ CDW state on the Sb-terminated surface was identified in our STM measurements (yellow circles in Figure 5d). It is further revealed by other groups that the superlattice also has a *c*-axis component, i.e., a 3D CDW with a $2\text{a} \times 2\text{a} \times 2\text{c}$ pattern, according to STM, X-ray scattering, and nuclear magnetic resonance experiments.^{43–45} The emergence of CDW is closely related to the van Hove singularities at *M* points near E_F . Particularly, a strip-like unidirectional superstructure with a $4\text{a} \times 1\text{a}$ vector has also been distinguished (orange circles in Figure 5d). The two types of CDW orders were both revealed in RbV_3Sb_5 , while the latter $4\text{a} \times 1\text{a}$ superlattice was absent in KV_3Sb_5 . Recently, various CDW states were also observed in kagome antiferromagnet FeGe and paramagnet ScV_6Sn_6 .^{46,47} These studies provide meaningful guidance for exploring and understanding the CDW and nontrivial band topology in kagome systems.

It is generally acknowledged that high pressure has served as a clean and effective technique to tune *in situ* the crystal and electronic structure, with the expectation of realizing novel quantum phenomena. The peculiar AV_3Sb_5 compounds provide an ideal platform to investigate the evolution and relationship between superconductivity and CDW by utilizing high pressure. One can see that the electrical responses are very evident under the application of pressure (Figures 5e and 5f). As shown in the T – P phase diagrams, T_{CDW} shows a rapid and monotonic decrease, while the superconducting transition temperature T_c exhibits superconducting domes under the pressure up to 50.7 GPa and attains the maximum value (8.2 K) at ~ 1 GPa. With increasing pressure, superconductivity first disappears at 13.1 GPa and surprisingly re-enters a superconducting state above 15 GPa. In the whole pressure region,

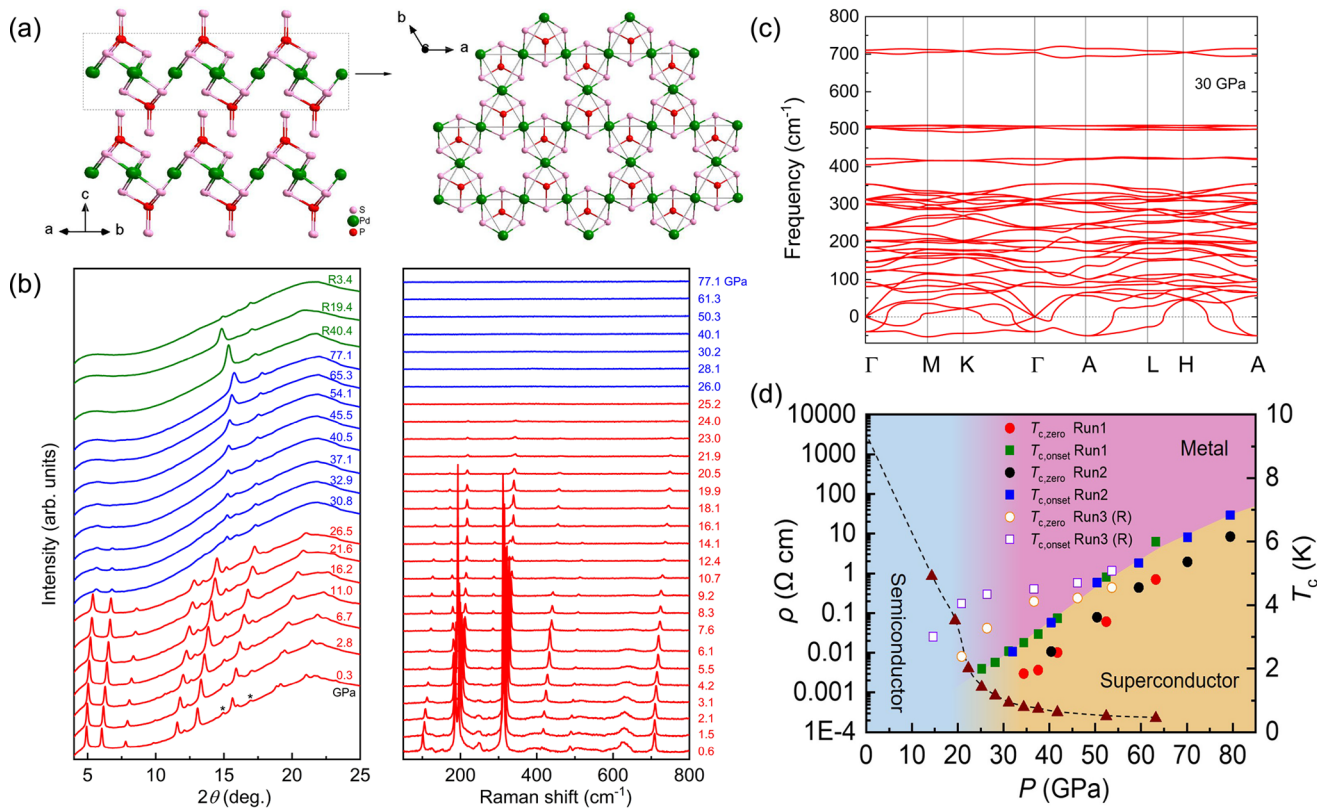


Figure 6. (a) Crystal structure of $\text{Pd}_3\text{P}_2\text{S}_8$. (b) High-pressure synchrotron radiation XRD patterns (left) and Raman spectra (right). The asterisks display the diffraction peaks of rhenium gasket, which arise from the trailing of the X-ray spot. R denotes the process of releasing pressure. (c) Phonon spectrum of $\text{Pd}_3\text{P}_2\text{S}_8$ at 30 GPa. (d) Phase diagram of $\text{Pd}_3\text{P}_2\text{S}_8$ under pressure. The values of resistivity ρ are taken at 10 K. Reproduced with permission from ref 55. Copyright 2023 IOP.

no structural phase transition is revealed. The enhancement of superconductivity at low pressures arises from the strongly competitive relation with the CDW state. Upon compression, the decrease of displacements of Sb₂ atoms is possibly responsible for the suppression of CDW order. Moreover, the emergence of the second superconducting state is closely associated with the changes in electronic structure. The dome-shaped superconducting behaviors have also emerged in RbV_3Sb_5 and KV_3Sb_5 .

Due to the weak interlayer interaction, the layered kagome structure is easier to mechanically exfoliate. It is found that T_c shows a nonmonotonic dependence on the thickness in CsV_3Sb_5 .⁴⁸ Nonreciprocal charge transport behaviors were observed in CsV_3Sb_5 thin flakes, exhibiting pronounced second harmonic signals in the superconducting state. It may be related to the intrinsic symmetry breaking arising from the unconventional superconducting state.

Although in the absence of magnetic order in AV_3Sb_5 , Ali's group reported that there is a large AHC in KV_3Sb_5 .⁴⁹ The chiral CDW breaking the time-reversal symmetry is possibly associated with the emergence of AHE.⁵⁰ In addition, more intriguing correlated phenomena have been successively reported by other groups, such as pair density wave, nematic phase, quantum transport, 2-fold symmetry of resistivity, etc.^{51–54}

3.2. $\text{Pd}_3\text{P}_2\text{S}_8$

Another kind of nonmagnetic kagome material is the van der Waals (vdW) compound $\text{Pd}_3\text{P}_2\text{S}_8$, which features a pristine Pd kagome lattice without other atom occupations (Figure 6a).⁵⁵

Similarly to AV_3Sb_5 , $\text{Pd}_3\text{P}_2\text{S}_8$ with weak interlayer vdW interactions can be easily cleaved into thin layers, even monolayers.⁵⁶ Nevertheless, $\text{Pd}_3\text{P}_2\text{S}_8$ is a semiconductor possessing an energy gap of 1.4–1.8 eV at ground state.^{56,57}

Due to the intrinsic semiconducting characteristics, it is expected to tune the physical properties by means of high pressure or chemical doping. High-pressure electrical transport studies revealed that the semiconducting behavior can be gradually suppressed, ultimately transitioning into a metallic state at 34.4 GPa (Figure 6d). Simultaneously, the superconductivity is successfully induced in the pressurized $\text{Pd}_3\text{P}_2\text{S}_8$. The T_c increases monotonously with pressure, and a maximum and unsaturated T_c of 6.83 K is obtained within the limit of our research. The almost vanishing strength of peaks above 26 GPa in both synchrotron radiation XRD and Raman spectroscopy suggest the occurrence of an amorphous phase transition when $\text{Pd}_3\text{P}_2\text{S}_8$ enters into the superconducting state (Figure 6b). Accordingly, the emergence of pressure-induced superconductivity is closely related to the amorphous phase. The calculated phonon spectra of $\text{Pd}_3\text{P}_2\text{S}_8$ reveal the presence of imaginary modes above 20 GPa (Figure 6c), confirming the structural instability under high pressure in the superconducting state. Upon compression, the sharp decrease of the distance between interlayer Pd and S atoms significantly enhances the interlayer coupling, and the crystal structure can be easily tuned into 3D and may become unstable. On the other hand, with Se doping at the S sites, the semiconducting ground state remains robust despite a gradual decrease of the band gap caused by the enhanced interlayer coupling.⁵⁷

4. SUMMARY AND OUTLOOK

Kagome lattice is a fantastic geometrical structure, which contains a variety of intriguing physical characteristics. It provides an excellent platform to study the exotic magnetism, quantum states, nontrivial topological properties, and correlation effects. Here, we have reviewed the progress on the representative topological quantum materials with magnetic/nonmagnetic kagome lattice. From the perspective of transport behaviors of conduction electrons, combined with the theoretical calculations and spectroscopic measurements, various striking quantum phenomena have been revealed, such as momentum/real-space Berry phase-driven giant electromagnetic responses including AHE and THE, enhanced and even induced superconductivity under pressure, CDW states, negative flat band magnetism, and tunable local magnetism. Our works undoubtedly enrich the variety of the kagome material family and provide insight into the understanding of strong entanglement between frustration, topology, and correlation.

Benefiting from the unique layered structure of kagome materials, it also provides a promising platform to explore low-dimensional physical performances. Although the most recently investigated kagome magnets tend to exhibit 3D bulk characteristics owing to the strong interlayer interactions, the nonmagnetic kagome materials like AV_3Sb_5 and $\text{Pd}_3\text{P}_2\text{S}_8$ can be easily exfoliated down to a few layers or a single layer. In the 2D limit, multiple experimental techniques, such as mechanical exfoliation, ionic liquid gating, intercalation, etc., can be utilized to manipulate the quantum states and discover novel physical phenomena. For example, by modulating the thickness of the film, it is expected to investigate the thickness-dependent AHE in kagome materials, including the varying magnitude of AHE and the evolution of the dominant mechanism. The dimensionality may also produce other exotic responses of kagome systems, such as the enhancement of superconductivity. Furthermore, the physical properties could also be modified through ionic liquid gating or intercalation, accompanied by the tuning of carrier densities, as well as the size and shape of the Fermi surface.

Theoretical calculations proposed that 2D kagome lattice with breaking time-reversal symmetry caused by magnetic order can realize a quantum anomalous Hall effect (QAHE) when the electron filling is within the gap. Magnetic Weyl semimetals including $\text{Co}_3\text{Sn}_2\text{S}_2$, $\text{Co}_3\text{Pb}_2\text{S}_2$, $\text{Co}_3\text{Pb}_2\text{Se}_2$, and $\text{Co}_3\text{Sn}_2\text{Se}_2$ were predicted to manifest nonzero Chern numbers and chiral edge states in the 2D limit, where Weyl points are broken and an energy gap opens.^{58,59} However, due to the difficulties in experimentally achieving an isolated magnetic 2D kagome layer, the QAHE accessing quantized AHC has not yet been observed in real kagome materials. In the future, the discovery of the suitable 2D magnetic kagome materials holds the promise of realizing this scenario. Moreover, the achievement of the quantized Hall effect enables to possess a large anomalous Hall angle $\sim 90^\circ$.

The effects of topological Dirac/Weyl fermions on the transport properties have been intensively studied. Currently, the related investigations of natural flat bands in the aspect of electrical properties are still sparse. Especially, the theoretically predicted superconductivity associated with flat bands has not been realized in kagome materials, although flat bands near E_F are revealed in FeSn and CoSn. The appropriate position of flat bands close to E_F with certain electron-electron

correlations may be vitally important for the presence of superconducting states, and further studies are still needed.

In conclusion, the exploration of novel topological quantum materials with kagome lattice are now becoming intriguing and promising. In the future, more striking quantum properties are expected to be excavated and studied. It will undoubtedly promote the development of the emerging topological matters and the application in the fields of spintronics devices, quantum computation, and so on.

■ AUTHOR INFORMATION

Corresponding Authors

Yanpeng Qi – *School of Physical Science and Technology, ShanghaiTech Laboratory for Topological Physics, and Shanghai Key Laboratory of High-Resolution Electron Microscopy, ShanghaiTech University, Shanghai 201210, China; orcid.org/0000-0003-2722-1375; Email: qyip@shanghaitech.edu.cn*

Hechang Lei – *Department of Physics and Beijing Key Laboratory of Optoelectronic Functional Materials & Micro-Nano Devices and Key Laboratory of Quantum State Construction and Manipulation (Ministry of Education), Renmin University of China, Beijing 100872, China; Email: hlei@ruc.edu.cn*

Authors

Qi Wang – *School of Physical Science and Technology and ShanghaiTech Laboratory for Topological Physics, ShanghaiTech University, Shanghai 201210, China; Department of Physics and Beijing Key Laboratory of Optoelectronic Functional Materials & Micro-Nano Devices, Renmin University of China, Beijing 100872, China; orcid.org/0000-0002-9599-7848*

Claudia Felser – *Max Planck Institute for Chemical Physics of Solids, Dresden 01187, Germany*

Complete contact information is available at:
<https://pubs.acs.org/10.1021/accountsrm.3c00291>

Notes

The authors declare no competing financial interest.

Biographies

Qi Wang gained her Ph.D. degree from the Renmin University of China in 2020. She is currently an assistant researcher at ShanghaiTech Laboratory for Topological Physics, ShanghaiTech University. Her research interests mainly focus on the exploration of novel topological materials and the studies of physical properties under extreme conditions (ultra-low temperature, strong field, and high pressure), including the anomalous Hall effect, the topological Hall effect, and superconductivity.

Hechang Lei obtained his Ph.D. degree from Institute of Solid State of Physics, Chinese Academy of Sciences in 2009. Now, he is a professor at the Department of Physics, Renmin University of China. His present research interests mainly focus on the exploration of exotic correlated topological matter and low-dimensional strongly correlated phenomena, such as superconductivity, frustrated magnetism, and other emergent low-dimensional quantum matter.

Yanpeng Qi obtained his Ph.D. degree from the Institute of Electrical Engineering, Chinese Academy of Sciences in 2011. Now, he is an assistant professor at the School of Physical Science and Technology, ShanghaiTech University. His current research interest focuses on the

understanding of novel properties of quantum materials under high pressures and the design and synthesis of new superconductors.

Claudia Felser is currently director at the Max Planck Institute for Chemical Physics of Solids in Dresden (Germany). Her research foci are the design and discovery of novel inorganic compounds, in particular, Heusler compounds for multiple applications and new topological quantum materials.

ACKNOWLEDGMENTS

This work was supported by the National Key R&D Program of China (Grants 2023YFA1607400, 2018YFA0704300, 2022YFA1403800, and 2023YFA1406500), the National Natural Science Foundation of China (Grants 52272265 and 12274459), the Shanghai Sailing Program (Grant 23YF1426800), and the Beijing Natural Science Foundation (Grant Z200005).

REFERENCES

- (1) Qi, X.-L.; Zhang, S.-C. Topological insulators and superconductors. *Rev. Mod. Phys.* **2011**, *83*, 1057.
- (2) Bansil, A.; Lin, H.; Das, T. Colloquium: Topological band theory. *Rev. Mod. Phys.* **2016**, *88*, No. 021004.
- (3) Xie, Y.; Chen, L.; Chen, T.; Wang, Q.; Yin, Q.; Stewart, J. R.; Stone, M. B.; Daemen, L. L.; Feng, E.; Cao, H.; Lei, H.; Yin, Z.; MacDonald, A. H.; Dai, P. Spin excitations in metallic kagome lattice FeSn and CoSn. *Commun. Phys.* **2021**, *4*, 240.
- (4) Hall, E. H. On a new action of the magnet on electric currents. *Am. J. Math.* **1879**, *2*, 287.
- (5) Hall, E. H. On the new action of magnetism on a permanent electric current. *Philos. Mag.* **1880**, *10*, 301.
- (6) Hall, E. H. On the “Rotational coefficient” in nickel and cobalt. *Philos. Mag.* **1881**, *12*, 157.
- (7) Karplus, R.; Luttinger, J. M. Hall effect in ferromagnetics. *Phys. Rev.* **1954**, *95*, 1154.
- (8) Jungwirth, T.; Niu, Q.; MacDonald, A. H. Anomalous Hall Effect in Ferromagnetic Semiconductors. *Phys. Rev. Lett.* **2002**, *88*, No. 207208.
- (9) Smit, J. The spontaneous Hall effect in ferromagnetics II. *Physica* **1958**, *24*, 39.
- (10) Berger, L. Side-jump mechanism for the Hall effect of ferromagnets. *Phys. Rev. B* **1970**, *2*, 4559.
- (11) Ueda, K.; Iguchi, S.; Suzuki, T.; Ishiwata, S.; Taguchi, Y.; Tokura, Y. Topological Hall Effect in Pyrochlore Lattice with Varying Density of Spin Chirality. *Phys. Rev. Lett.* **2012**, *108*, No. 156601.
- (12) Tang, E.; Mei, J. W.; Wen, X. G. High Temperature Fractional Quantum Hall States. *Phys. Rev. Lett.* **2011**, *106*, No. 236802.
- (13) Wang, W.-S.; Li, Z.-Z.; Xiang, Y.-Y.; Wang, Q.-H. Competing electronic orders on kagome lattices at van Hove filling. *Phys. Rev. B* **2013**, *87*, No. 115135.
- (14) Wang, Q.; Sun, S. S.; Zhang, X.; Pang, F.; Lei, H. C. Anomalous Hall effect in a ferromagnetic Fe₃Sn₂ single crystal with a geometrically frustrated Fe bilayer kagome lattice. *Phys. Rev. B* **2016**, *94*, No. 075135.
- (15) Fenner, L. A.; Dee, A. A.; Wills, A. S. Non-collinearity and spin frustration in the itinerant kagome ferromagnet Fe₃Sn₂. *J. Phys.: Condens. Matter* **2009**, *21*, No. 452202.
- (16) Ye, L.; Kang, M.; Liu, J.; von Cube, F.; Wicker, C. R.; Suzuki, T.; Jozwiak, C.; Bostwick, A.; Rotenberg, E.; Bell, D. C.; Fu, L.; Comin, R.; Checkelsky, J. G. Massive Dirac fermions in a ferromagnetic kagome metal. *Nature* **2018**, *555*, 638.
- (17) Neubauer, A.; Pfleiderer, C.; Binz, B.; Rosch, A.; Ritz, R.; Niklowitz, P. G.; Boni, P. Topological Hall Effect in the A Phase of MnSi. *Phys. Rev. Lett.* **2009**, *102*, No. 186602.
- (18) Kurumaji, T.; Nakajima, T.; Hirschberger, M.; Kikkawa, A.; Yamasaki, Y.; Sagayama, H.; Nakao, H.; Taguchi, Y.; Arima, T.; Tokura, Y. Skyrmiion lattice with a giant topological Hall effect in a frustrated triangular-lattice magnet. *Science* **2019**, *365*, 914.
- (19) Hou, Z.; Ren, W.; Ding, B.; Xu, G.; Wang, Y.; Yang, B.; Zhang, Q.; Zhang, Y.; Liu, E.; Xu, F.; Wang, W.; Wu, G.; Zhang, X.; Shen, B.; Zhang, Z. Observation of Various and Spontaneous Magnetic Skyrmionic Bubbles at Room Temperature in a Frustrated Kagome Magnet with Uniaxial Magnetic Anisotropy. *Adv. Mater.* **2017**, *29*, No. 1701144.
- (20) Wang, Q.; Yin, Q. W.; Lei, H. C. Giant topological Hall effect of ferromagnetic kagome metal Fe₃Sn₂. *Chin. Phys. B* **2020**, *29*, No. 017101.
- (21) Li, Y.; Wang, Q.; DeBeer-Schmitt, L.; Guguchia, Z.; Desautels, R. D.; Yin, J.-X.; Du, Q.; Ren, W.; Zhao, X.; Zhang, Z.; Zaliznyak, I. A.; Petrovic, C.; Yin, W.; Hasan, M. Z.; Lei, H.; Tranquada, J. M. Magnetic-field Control of Topological Electronic Response near Room Temperature in Correlated Kagome Magnets. *Phys. Rev. Lett.* **2019**, *123*, No. 196604.
- (22) Lin, Z.; Choi, J.-H.; Zhang, Q.; Qin, W.; Yi, S.; Wang, P.; Li, L.; Wang, Y.; Zhang, H.; Sun, Z.; Wei, L.; Zhang, S.; Guo, T.; Lu, Q.; Cho, J.-H.; Zeng, C.; Zhang, Z. Flatbands and Emergent Ferromagnetic Ordering in Fe₃Sn₂ Kagome Lattices. *Phys. Rev. Lett.* **2018**, *121*, No. 096401.
- (23) Wan, X.; Turner, A. M.; Vishwanath, A.; Savrasov, S. Y. Topological semimetal and Fermi arc surface states in the electronic structure of pyrochlore iridates. *Phys. Rev. B* **2011**, *83*, No. 205101.
- (24) Xu, G.; Weng, H.; Wang, Z.; Dai, X.; Fang, Z. Chern semimetal and the quantized anomalous Hall effect in HgCr₂Se₄. *Phys. Rev. Lett.* **2011**, *107*, No. 186806.
- (25) Wang, Q.; Xu, Y. F.; Lou, R.; Liu, Z.; Li, M.; Huang, Y.; Shen, D.; Weng, H. M.; Wang, S. C.; Lei, H. C. Large intrinsic anomalous Hall effect in halfmetallic ferromagnet Co₃Sn₂S₂ with magnetic Weyl fermions. *Nat. Commun.* **2018**, *9*, 3681.
- (26) Liu, E.; Sun, Y.; Kumar, N.; Muechler, L.; Sun, A.; Jiao, L.; Yang, S. Y.; Liu, D.; Liang, A.; Xu, Q.; Kroder, J.; Süß, V.; Borrmann, H.; Shekhar, C.; Wang, Z.; Xi, C.; Wang, W.; Schnelle, W.; Wirth, S.; Chen, Y.; Goennenwein, S. T. B.; Felser, C. Giant anomalous Hall effect in a ferromagnetic kagome-lattice semimetal. *Nat. Phys.* **2018**, *14*, 1125.
- (27) Liu, D. F.; Liang, A. J.; Liu, E. K.; Xu, Q. N.; Li, Y. W.; Chen, C.; Pei, D.; Shi, W. J.; Mo, S. K.; Dudin, P.; Kim, T.; Cacho, C.; Li, G.; Sun, Y.; Yang, X. L.; Liu, Z. K.; Parkin, S. S. P.; Felser, C.; Chen, Y. L. Magnetic Weyl semimetal phase in a Kagome crystal. *Science* **2019**, *365*, 1282.
- (28) Morali, N.; Batabyal, R.; Nag, P. K.; Liu, E.; Xu, Q.; Sun, Y.; Yan, B.; Felser, C.; Avraham, N.; Beidenkopf, H. Fermi-arc diversity on surface terminations of the magnetic Weyl semimetal Co₃Sn₂S₂. *Science* **2019**, *365*, 1286.
- (29) Yin, J. X.; Zhang, S. S.; Chang, G. Q.; Wang, Q.; Tsirkin, S. S.; Guguchia, Z.; Lian, B.; Zhou, H.; Jiang, K.; Belopolski, I.; Shumiya, N.; Multer, D.; Litskevich, M.; Cochran, T. A.; Lin, H.; Wang, Z.; Neupert, T.; Jia, S.; Lei, H. C.; Hasan, M. Z. Negative flat band magnetism in a spin-orbit-coupled correlated kagome magnet. *Nat. Phys.* **2019**, *15*, 443.
- (30) Wang, Q.; Neubauer, K. J.; Duan, C.; Yin, Q. W.; Fujitsu, S.; Hosono, H.; Ye, F.; Zhang, R.; Chi, S.; Krycka, K.; Lei, H. C.; Dai, P. C. Field-induced topological Hall effect and double-fan spin structure with a c-axis component in the metallic kagome antiferromagnetic compound YMn₆Sn₆. *Phys. Rev. B* **2021**, *103*, No. 014416.
- (31) Ma, W.; Xu, X.; Yin, J.-X.; Yang, H.; Zhou, H.; Cheng, Z.-J.; Huang, Y.; Qu, Z.; Wang, F.; Hasan, M. Z.; Jia, S. Rare Earth Engineering in RMn₆Sn₆ (R = Gd-Tm, Lu). *Phys. Rev. Lett.* **2021**, *126*, No. 246602.
- (32) Yin, J.-X.; Ma, W.; Cochran, T. A.; Xu, X.; Zhang, S. S.; Tien, H.-J.; Shumiya, N.; Cheng, G.; Jiang, K.; Lian, B.; Song, Z.; Chang, G.; Belopolski, I.; Multer, D.; Litskevich, M.; Cheng, Z.-J.; Yang, X. P.; Swidler, B.; Zhou, H.; Lin, H.; Neupert, T.; Wang, Z.; Yao, N.; Chang, T.-R.; Jia, S.; Zahid Hasan, M. Quantum-limit Chern topological magnetism in TbMn₆Sn₆. *Nature* **2020**, *583*, 533.

- (33) Li, M.; Wang, Q.; Wang, G.; Yuan, Z.; Song, W.; Lou, R.; Liu, Z.; Huang, Y.; Liu, Z.; Lei, H. C.; Yin, Z. P.; Wang, S. C. Dirac cone, flat band and saddle point in kagome magnet YMn_6Sn_6 . *Nat. Commun.* **2021**, *12*, 3129.
- (34) Nakatsuji, S.; Kiyohara, N.; Higo, T. Large anomalous Hall effect in a non-collinear antiferromagnet at room temperature. *Nature* **2015**, *527*, 212.
- (35) Kuroda, K.; Tomita, T.; Suzuki, M.-T.; Bareille, C.; Nugroho, A. A.; Goswami, P.; Ochi, M.; Ikhlas, M.; Nakayama, M.; Akebi, S.; Noguchi, R.; Ishii, R.; Inami, N.; Ono, K.; Kumigashira, H.; Varykhalov, A.; Muro, T.; Koretsune, T.; Arita, R.; Shin, S.; Kondo, T.; Nakatsuji, S. Evidence for magnetic Weyl fermions in a correlated metal. *Nat. Mater.* **2017**, *16*, 1090.
- (36) Kang, M.; Ye, L.; Fang, S.; You, J.-S.; Levitan, A.; Han, M.; Facio, J. I.; Jozwiak, C.; Bostwick, A.; Rotenberg, E.; Chan, M. K.; McDonald, R. D.; Graf, D.; Kaznatcheev, K.; Vescovo, E.; Bell, D. C.; Kaxiras, E.; van den Brink, J.; Richter, M.; Prasad Ghimire, M.; Checkelsky, J. G.; Comin, R. Dirac fermions and flat bands in the ideal kagome metal FeSn . *Nat. Mater.* **2020**, *19*, 163.
- (37) Liu, Z.; Li, M.; Wang, Q.; Wang, G.; Wen, C.; Jiang, K.; Lu, X.; Yan, S.; Huang, Y.; Shen, D.; Yin, J.-X.; Wang, Z.; Yin, Z.; Lei, H. C.; Wang, S. C. Orbital-selective Dirac fermions and extremely flat bands in frustrated kagome-lattice metal CoSn . *Nat. Commun.* **2020**, *11*, 4002.
- (38) Yin, J. X.; Shumiya, N.; Mardanya, S.; Wang, Q.; Zhang, S. S.; Tien, H.-J.; Multer, D.; Jiang, Y.; Cheng, G.; Yao, N.; Wu, S.; Wu, D.; Deng, L.; Ye, Z.; He, R.; Chang, G.; Liu, Z.; Jiang, K.; Wang, Z.; Neupert, T.; Agarwal, A.; Chang, T.-R.; Chu, C.-W.; Lei, H. C.; Hasan, M. Z. Fermion-boson many-body interplay in a frustrated kagome paramagnet. *Nat. Commun.* **2020**, *11*, 4003.
- (39) Ortiz, B. R.; Gomes, L. C.; Morey, J. R.; Winiarski, M.; Bordelon, M.; Mangum, J. S.; Oswald, I. W. H.; Rodriguez-Rivera, J. A.; Neilson, J. R.; Wilson, S. D.; Ertekin, E.; McQueen, T. M.; Toberer, E. S. New kagome prototype materials: discovery of KV_3Sb_5 , RbV_3Sb_5 , and CsV_3Sb_5 . *Phys. Rev. Mater.* **2019**, *3*, No. 094407.
- (40) Ortiz, B. R.; Teicher, S. M. L.; Hu, Y.; Zuo, J. L.; Sarte, P. M.; Schueller, E. C.; Abeykoon, A. M. M.; Krogstad, M. J.; Rosenkranz, S.; Osborn, R.; Seshadri, R.; Balents, L.; He, J.; Wilson, S. D. CsV_3Sb_5 : A Z_2 Topological Kagome Metal with a Superconducting Ground State. *Phys. Rev. Lett.* **2020**, *125*, No. 247002.
- (41) Yin, Q. W.; Tu, Z. J.; Gong, C. S.; Fu, Y.; Yan, S. H.; Lei, H. C. Superconductivity and Normal-State Properties of Kagome Metal RbV_3Sb_5 Single Crystals. *Chin. Phys. Lett.* **2021**, *38*, No. 037403.
- (42) Wang, Q.; Kong, P.; Shi, W.; Pei, C.; Wen, C.; Gao, L.; Zhao, Y.; Yin, Q.; Wu, Y.; Li, G.; Lei, H. C.; Li, J.; Chen, Y. L.; Yan, S. C.; Qi, Y. P. Charge Density Wave Orders and Enhanced Superconductivity under Pressure in the Kagome Metal CsV_3Sb_5 . *Adv. Mater.* **2021**, *33*, No. 2102813.
- (43) Liang, Z.; Hou, X.; Zhang, F.; Ma, W.; Wu, P.; Zhang, Z.; Yu, F.; Ying, J.-J.; Jiang, K.; Shan, L.; Wang, Z.; Chen, X.-H. Three-Dimensional Charge Density Wave and Surface-Dependent Vortex-Core States in a Kagome Superconductor CsV_3Sb_5 . *Phys. Rev. X* **2021**, *11*, No. 031026.
- (44) Li, H.; Zhang, T. T.; Yilmaz, T.; Pai, Y. Y.; Marvinney, C. E.; Said, A.; Yin, Q. W.; Gong, C. S.; Tu, Z. J.; Vescovo, E.; Nelson, C. S.; Moore, R. G.; Murakami, S.; Lei, H. C.; Lee, H. N.; Lawrie, B. J.; Miao, H. Observation of Unconventional Charge Density Wave without Acoustic Phonon Anomaly in Kagome Superconductors AV_3Sb_5 ($\text{A} = \text{Rb}, \text{Cs}$). *Phys. Rev. X* **2021**, *11*, No. 031050.
- (45) Song, D.; Zheng, L.; Yu, F.; Li, J.; Nie, L.; Shan, M.; Zhao, D.; Li, S. J.; Kang, B. L.; Wu, Z. M.; Zhou, Y. B.; Sun, K. L.; Liu, K.; Luo, X. G.; Wang, Z. Y.; Ying, J. J.; Wan, X. G.; Wu, T.; Chen, X. H. Orbital ordering and fluctuations in a kagome superconductor CsV_3Sb_5 . *Sci. China Phys. Mech. Astron.* **2022**, *65*, No. 247462.
- (46) Teng, X.; Chen, L.; Ye, F.; Rosenberg, E.; Liu, Z.; Yin, J.-X.; Jiang, Y.-X.; Oh, J. S.; Hasan, M. Z.; Neubauer, K. J.; Gao, B.; Xie, Y.; Hashimoto, M.; Lu, D.; Jozwiak, C.; Bostwick, A.; Rotenberg, E.; Birgeneau, R. J.; Chu, J.-H.; Yi, M.; Dai, P. Discovery of charge density wave in a kagome lattice antiferromagnet. *Nature* **2022**, *609*, 490.
- (47) Arachchige, H. W. S.; Meier, W. R.; Marshall, M.; Matsuoka, T.; Xue, R.; McGuire, M. A.; Hermann, R. P.; Cao, H.; Mandrus, D. Charge Density Wave in Kagome Lattice Intermetallic ScV_6Sn_6 . *Phys. Rev. Lett.* **2022**, *129*, No. 216402.
- (48) Wu, Y.; Wang, Q.; Zhou, X.; Wang, J.; Dong, P.; He, J.; Ding, Y.; Teng, B.; Zhang, Y.; Li, Y.; Zhao, C.; Zhang, H.; Liu, J.; Qi, Y. P.; Watanabe, K.; Taniguchi, T.; Li, J. Nonreciprocal Charge Transport in Topological Kagome Superconductor CsV_3Sb_5 . *npj Quantum Mater.* **2022**, *7*, 105.
- (49) Yang, S.-Y.; Wang, Y.; Ortiz, B. R.; Liu, D.; Gayles, J.; Derunova, E.; Gonzalez-Hernandez, R.; Smejkal, L.; Chen, Y.; Parkin, S. S. P.; Wilson, S. D.; Toberer, E. S.; McQueen, T.; Ali, M. N. Giant, unconventional anomalous Hall effect in the metallic frustrated magnet candidate, KV_3Sb_5 . *Sci. Adv.* **2020**, *6*, No. eabb6003.
- (50) Jiang, Y.-X.; Yin, J.-X.; Denner, M. M.; Shumiya, N.; Ortiz, B. R.; Xu, G.; Guguchia, Z.; He, J.; Hossain, M. S.; Liu, X.; Ruff, J.; Kautzsch, L.; Zhang, S. S.; Chang, G.; Belopolski, I.; Zhang, Q.; Cochran, T. A.; Multer, D.; Litskevich, M.; Cheng, Z.-J.; Yang, X. P.; Wang, Z.; Thomale, R.; Neupert, T.; Wilson, S. D.; Hasan, M. Z. Unconventional chiral charge order in kagome superconductor KV_3Sb_5 . *Nat. Mater.* **2021**, *20*, 1353.
- (51) Chen, H.; Yang, H.; Hu, B.; Zhao, Z.; Yuan, J.; Xing, Y.; Qian, G.; Huang, Z.; Li, G.; Ye, Y.; Ma, S.; Ni, S.; Zhang, H.; Yin, Q.; Gong, C.; Tu, Z.; Lei, H.; Tan, H.; Zhou, S.; Shen, C.; Dong, X.; Yan, B.; Wang, Z.; Gao, H.-J. Roton pair density wave in a strong-coupling kagome superconductor. *Nature* **2021**, *599*, 222.
- (52) Nie, L.; Sun, K.; Ma, W.; Song, D.; Zheng, L.; Liang, Z.; Wu, P.; Yu, F.; Li, J.; Shan, M.; Zhao, D.; Li, S.; Kang, B.; Wu, Z.; Zhou, Y.; Liu, K.; Xiang, Z.; Ying, J.; Wang, Z.; Wu, T.; Chen, X. H. Charge-density-wave-driven electronic nematicity in a kagome superconductor. *Nature* **2022**, *604*, 59.
- (53) Fu, Y.; Zhao, N.; Chen, Z.; Yin, Q.; Tu, Z.; Gong, C.; Xi, C.; Zhu, X.; Sun, Y.; Liu, K.; Lei, H. Quantum Transport Evidence of Topological Band Structures of Kagome Superconductor CsV_3Sb_5 . *Phys. Rev. Lett.* **2021**, *127*, No. 207002.
- (54) Xiang, Y.; Li, Q.; Li, Y.; Xie, W.; Yang, H.; Wang, Z.; Yao, Y.; Wen, H.-H. Twofold symmetry of c -axis resistivity in topological kagome superconductor CsV_3Sb_5 with in-plane rotating magnetic field. *Nat. Commun.* **2021**, *12*, 6727.
- (55) Wang, Q.; Qiu, X.-L.; Pei, C.; Gong, B.-C.; Gao, L.; Zhao, Y.; Cao, W.; Li, C.; Zhu, S.; Zhang, M.; Chen, Y. L.; Liu, K.; Qi, Y. P. Superconductivity emerging from a pressurized van der Waals kagome material $\text{Pd}_3\text{P}_2\text{S}_8$. *New J. Phys.* **2023**, *25*, No. 043001.
- (56) Park, S.; Kang, S.; Kim, H.; Lee, K. H.; Kim, P.; Sim, S.; Lee, N.; Karuppannan, B.; Kim, J.; Kim, J.; Sim, K. I.; Coak, M. J.; Noda, Y.; Park, C.-H.; Kim, J. H.; Park, J.-G. Kagome van-der-Waals $\text{Pd}_3\text{P}_2\text{S}_8$ with flat band. *Sci. Rep.* **2020**, *10*, No. 20998.
- (57) Yan, S.; Gong, B.-C.; Wang, L.; Wu, J.; Yin, Q.; Cao, X.; Zhang, X.; Liu, X.; Lu, Z.-Y.; Liu, K.; Lei, H. C. Evolution of ultraflat band in the van der Waals kagome semiconductor $\text{Pd}_3\text{P}_2(\text{S}_{1-x}\text{Se}_x)_8$. *Phys. Rev. B* **2022**, *105*, No. 155115.
- (58) Muechler, L.; Liu, E.; Gayles, J.; Xu, Q.; Felser, C.; Sun, Y. Emerging chiral edge states from the confinement of a magnetic Weyl semimetal in $\text{Co}_3\text{Sn}_2\text{S}_2$. *Phys. Rev. B* **2020**, *101*, No. 115106.
- (59) Zhang, Z.; You, J.-Y.; Ma, X.-Y.; Gu, B.; Su, G. Kagome quantum anomalous Hall effect with high Chern number and large band gap. *Phys. Rev. B* **2021**, *103*, No. 014410.